THE JOURNAL OF PHYSICAL CHEMISTRY A

Article

pubs.acs.org/JPCA

UV Absorption Spectrum of Alternating DNA Duplexes. Analysis of Excitonic and Charge Transfer Interactions

Felix Plasser,*[,†] Adelia J. A. Aquino,[‡,§] William L. Hase,[§] and Hans Lischka*[,†,§]

[†]Institute of Theoretical Chemistry, University of Vienna, Währingerstrasse 17, A-1090, Vienna, Austria

[‡]Institute of Soil Research, University of Natural Resources and Life Sciences, Peter-Jordan-Strasse 82, A-1190, Vienna, Austria

[§]Department of Chemistry and Biochemistry, Texas Tech University, Lubbock, Texas 79409-1061, United States

Supporting Information

ABSTRACT: A detailed investigation of the excited states accessed by UV absorption in alternating DNA duplexes was performed by means of an extensive sampling of intra- and intermolecular degrees of freedom. The excited states were computed using the algebraic diagrammatic construction method to second-order (ADC(2)). A realistic DNA environment was included through an electrostatic embedding QM/MM coupling scheme. The results indicate that (i) most excited states are delocalized over at most two bases, (ii) charge transfer states are located at higher energies than the bright states in the Franck−Condon region, but (iii) coupling between locally excited and charge transfer states may provide a route to dynamical charge separation, and (iv) spectral broadening is mainly caused by intramolecular vibrations.

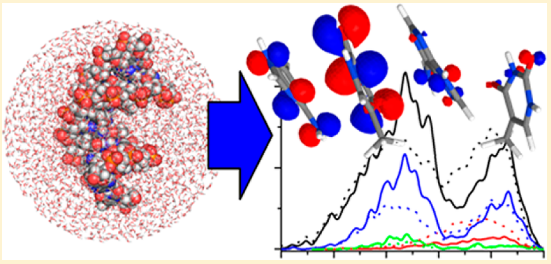

1. INTRODUCTION

Deoxyribonucleic acid (DNA) plays a central role in biology as the carrier of the genetic code. Absorption of UV light can potentially damage DNA leading to mutations, genomic instability or carcinogenesis.[1] A major defense mechanism against these possibilities is based on ultrafast decay, converting the electronic excitation energy into hot vibrational motion in the ground state.[2−9] When the photophysics of DNA are studied, the collective behavior and interactions between nucleobases are considered to play a decisive role. Whereas isolated nucleobases decay on a picosecond time scale, single and double stranded DNA show additional transients with a 10−100 ps lifetime and even nano second components were found.[8,10−14] Both excitonic delocalization[12,13,15−18] and interbase charge transfer[10,19−21] are being considered as processes arising due to base−base interactions, which may be responsible for the above-mentioned change in dynamical behavior. A wide range of different results concerning excitonic delocalization has been reported. In single-stranded homo-adenine polymers the delocalization was estimated at around three bases and it was pointed out that delocalization should be smaller in alternating sequences.[12,20,22] A computational study reported excitonic delocalization of at least two bases in dCdG polymers.[23] In contrast to these estimates of rather small delocalization degrees, parametrized exciton theory yielded significantly larger estimates of six bases and more for poly dA and poly dGdC.[16,18] Moreover, from time-dependent fluorescence anisotropy studies on different base sequences, possible signatures of excitonic dynamics and excitation energy transfer between the bases were reported.[13,15,18] The existence of charge transfer states, on the other hand, is considered of highest importance as well, as they may lead to exciplexes that could act as trapping sites.[8,10] In this case there is some discrepancy as far as their energetic ordering with respect to the bright states is concerned. Studies using time-dependent density functional theory (TDDFT) tended to place charge transfer states at lower or comparable energies as the bright states[24,25] or just above the $\pi-\pi^*$ excitonic bright states,[20] whereas they were found at somewhat higher energies in wave function based ab initio studies.[17,26]

Even though the role of excitonic and charge transfer states has been discussed extensively in the literature, the information deduced from experiment is rather indirect and computational studies have the possibility to furnish a large amount of additional interesting information. Exciton theory, as one option (cf. refs 16, 23, 27, and 28), provides a convenient tool for modeling electronic spectra and dynamical processes. These studies gave interesting insight but require tedious investigations to obtain the necessary parametrization. These approaches concentrate on statistical broadening and static disorder and do not consider the explicit sampling of the many internal degrees of freedom in the system. Furthermore, the excitonic models considered only one or a few $\pi\pi^*$ states per monomer, ignoring mixing to other states of $\pi\pi^*$ or $n\pi^*$ character. Finally, an inclusion of charge transfer configurations is challenging within such an approach and was only performed

Special Issue: Jörn Manz Festschrift

Received: May 15, 2012
Revised: July 9, 2012
Published: July 11, 2012

   dx.doi.org/10.1021/jp304725r | J. Phys. Chem. A 2012, 116, 11151−11160

in one of these studies.[28] Compared to parametrized exciton theory, quantum chemical calculations on the excited states of particular molecular systems offer the possibility of including excitonic and charge transfer (CT) interactions at the same level in an integrated way based on well tested computational models. A number of different calculations on DNA fragments have been performed (cf. ref 29). The TDDFT approach, as one powerful option, allows treating DNA fragments efficiently[20,22,25] but care has to be taken in computing charge transfer states correctly[26,30,31] and special calibration is needed for obtaining accurate results.[20] In contrast to TDDFT, methods such as the second-order approximate coupled cluster model CC2[32] or algebraic diagrammatic construction to second-order ADC(2)[33] approaches offer the possibility of balanced calculations of excitonic and charge transfer states without any particular bias to either side. Additionally, usage of the resolution of the identity (RI)[34] approximation allows for efficient calculations on sufficiently large molecular systems to study stacking effects in the excited states. A systematic gas phase RI-CC2 study gave detailed insight into the different components of interbase coupling and other parameters,[35] and comparisons of different ab initio methods on stacked dimers in comparison to selected functionals used in TDDFT calculations were performed as well.[26,36] Water solvation in the QM calculations was included by explicit solvent[20] and by polarizable continuum methods.[25,26] Molecular dynamics simulations were performed for sampling purposes.[16,20,22,23,27] Moreover, it was shown that environmental fluctuations may lead to significant changes in orbital energies in DNA[37] and that in particular the CT states were sensitive to the particular water configuration.[20] Thus, an accurate treatment of the interplay between thermal flexibility and restrains from stacking interactions and the backbone is necessary to obtain accurate relative positions of DNA bases as this may affect the interbase coupling significantly.[16,35,36]

In this work a detailed computational analysis of the initial distribution of excited states in DNA accessed through UV absorption will be performed, where in particular the amount of excitonic delocalization and charge transfer will be considered. In the light of the above considerations, we designed our study to comply with the following points: (i) a reliable description of the excited states giving a balanced treatment of excitonic and CT interactions, (ii) a fully integrated description of the DNA environment, (iii) consistent sampling of intra- and intermolecular degrees of freedom, and (iv) development and application of methods to analyze the complex pattern of the excited-state wave functions. A QM/MM strategy has been adopted to address these points based on a DNA dodecamer (Figure 1). The QM part of the entire complex is computed at the ADC(2)[33] level with the strong advantages in terms of balanced description of excitonic and charge transfer states already mentioned above.

In the present simulations, the $(dAdT)_6{\cdot}(dAdT)_6$ and $(dGdC)_6{\cdot}(dGdC)_6$ alternating duplexes were chosen. The QM region consisted of two stacked bases (AT and GC, respectively) as well as four stacked bases (TATA, CGCG). Stacked bases rather than Watson–Crick paired bases were considered in light of experimental[8,10] and computational[25,28] evidence that the main interaction is between stacked bases along one strand. Moreover, interstrand CT was considered only important in homopolymeric sequences and located at higher energies in alternating duplexes.[20]

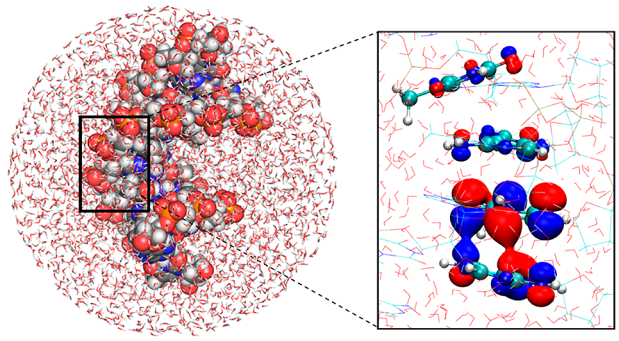

Figure 1. Depiction of the QM/MM methodology used in this work. Configurational sampling was performed by molecular dynamics simulations of a DNA dodecamer duplex solvated in a water droplet (left). ADC(2) calculations using electrostatic embedding were performed (right).

2. COMPUTATIONAL DETAILS

The electronic structure calculations were performed using the RI-ADC(2) method as implemented in the Turbomole 6.3 program package.[33,34,38,39] Calculations on selected structures were made with the SVP basis[40] for comparison reasons. Because of the relatively high computational cost for the sampling of the stacked dimer and tetramer structures on the order of 300–500 structures for each case as described below, the SV basis set[40] was used after verification against SVP results. In all calculations the core orbitals were frozen. In the tetramer spectra calculations the twenty lowest lying σ orbitals were frozen as well for reasons of computational efficiency. Test calculations described in the text below showed minor basis set effects on excitation energies on the order of 0.2 eV.

Base stacks in vacuo were arranged according to an ideal B helix configuration considering one strand. The vibrational broadening of the spectra was computed from the Wigner distribution of the harmonic intramolecular modes in the electronic ground state as described in ref 41. Reference dimer and tetramer structures, were extracted from an idealized B-DNA structure created with the Tinker nucleic program. The respective nucleobase structures were replaced by those optimized at the QM level in the ground state using a quaternion least-squares fit, cf. refs 42–44 (for the resulting geometries see the Supporting Information, Tables S3–S6). The Wigner distribution was computed from the harmonic frequencies for the dimer or tetramer, respectively, using the intramolecular modes only. Intermolecular motions, which will depend on a large number of low frequency anharmonic backbone vibrations, were excluded because they are not available in the isolated stacks. However, they will be included in the full DNA model. For computations in this full DNA model, mixed initial conditions following ref 45. were created. Intramolecular modes of the molecules in the QM region were treated at a quantum mechanical level using the Wigner distribution of normal modes. The modes of the backbone determining the relative positions of the bases and the environmental degrees of freedom were sampled by classical molecular dynamics (MD), considering the fact that for these strongly anharmonic low-frequency modes a Wigner sampling using harmonic modes is not adequate and, on the other hand, classical sampling is quite appropriate. For each of the structures selected from the dynamics simulations, the two and four nucleobases, respectively, obtained from the samples of the Wigner distribution of the individual bases in vacuo were

inserted at their appropriate places into the DNA structure using a quaternion least-squares fit. Then a 1 ps MD run was performed to relax the environment according to the small changes induced by the Wigner sample, whereas the structures and positions of the inserted bases were kept fixed. Finally, the atomic positions of the last MD step were used to perform a QM/MM calculation on the vertical excitation energies.

The inserted stacked dimer and tetramer, respectively, connected to the sugar/phosphate backbone using a link hydrogen atom techninque,[46,47] constituted the QM region and the remaining atoms were included in the QM/MM calculation by means of electrostatic embedding as point charges using their Amber-99 values. The charge of the carbon atom forming the link atom on the MM side was set to zero, and to maintain the original neutral charge of the overall system, the excess charge (i.e., the sum of the deleted charge of the MM-link atom and the partial charge corresponding to the atoms in the QM region) were equally distributed onto the three atoms bonded to the MM-link atom (cf. ref 48).

The computations in DNA were performed on $(dAdT)_6{\cdot}(dAdT)_6$ and $(dGdC)_6{\cdot}(dGdC)_6$ duplexes embedded in a sphere of 3000 water molecules, neutralized with 22 K^+ counterions. After creation of an initial structure using Packmol,[49] equilibration and sampling was performed by means of a classical molecular dynamics simulation using the Amber-99[50] force field, as implemented in Tinker.[51] Sampling was performed every 0.2 ps.

The spectra simulation was performed using the program system Newton-X.[41,52] A total of 300−500 distinct molecular geometries and environmental configurations were chosen. A phenomenological broadening of 0.05 eV was applied. Resulting distributions were normalized to put the different calculations on the same scale. For dimers ten excited states were computed, for tetramers twenty. The spectra were constructed considering vertical excitation energies and oscillator strengths at the displaced structures. In addition, a density of transitions (DOT) was computed. In this case, the same methodology as for the spectra, only with a formal unit oscillator strength, was used. For plotting, the density of transition was rescaled to have the same total area as the spectrum.

An automated analysis of the excited states was performed according to a recently developed scheme of analyzing the one-electron transition density matrix[53] using previous work by Tretiak[54] and Luzanov,[55] where specifically in the case of ADC(2) the singly excited cluster amplitudes were chosen to represent the transition density matrix (as explained in more detail in ref 53). This method provides well-defined descriptors for properties like the position, delocalization, and charge transfer character of the wave function even in difficult cases (e.g., delocalized orbitals, many contributing configurations). First, charge transfer numbers for an excited state α are computed

$$\Omega^{\alpha}_{\mathrm{AB}} = \frac{1}{2}\sum_{\substack{a\in \mathrm{A}\\ b\in \mathrm{B}}} (\mathbf{D}^{0\alpha,[\mathrm{AO}]}\mathbf{S}^{[\mathrm{AO}]})_{ab}(\mathbf{S}^{[\mathrm{AO}]}\mathbf{D}^{0\alpha,[\mathrm{AO}]})_{ab} \tag{1}$$

from the transition density matrix between this state and the ground state $\mathbf{D}^{0\alpha,[\mathrm{AO}]}$ and the overlap matrix $\mathbf{S}^{[\mathrm{AO}]}$, both expressed in the atomic orbital (AO) basis. The summations go over the basis functions on fragments A and B, respectively. Using the charge transfer numbers, the position (POS) of the exciton in the dimer or tetramer can be defined as

$$\mathrm{POS}^{\alpha} = \frac{\sum_{\mathrm{A}} A \sum_{\mathrm{B}} (\Omega^{\alpha}_{\mathrm{AB}} + \Omega^{\alpha}_{\mathrm{BA}})}{2\Omega^{\alpha}} \tag{2}$$

where the summation indices A and B go over the two or four molecules of the QM region and the symbol Ω^{α} is used to represent the normalization factor

$$\Omega^{\alpha} = \sum_{\mathrm{A,B}} \Omega^{\alpha}_{\mathrm{AB}} \tag{3}$$

For a state α localized only on one fragment C, i.e., $\Omega^{\alpha}_{\mathrm{CC}} = \Omega^{\alpha}$ and all other elements of the $\mathbf{\Omega}^{\alpha}$ matrix are vanishing, it follows that $\mathrm{POS}^{\alpha} = C$. For states that are distributed over several fragments, the POS^{α} value corresponds to the weighted average of the indices of theses fragments. The excitonic delocalization may be defined as a participation ratio (PR) expression

$$\mathrm{PR}^{\alpha} = \frac{(\Omega^{\alpha})^2}{2}\left(\frac{1}{\sum_{\mathrm{A}}(\sum_{\mathrm{B}}\Omega^{\alpha}_{\mathrm{AB}})^2} + \frac{1}{\sum_{\mathrm{B}}(\sum_{\mathrm{A}}\Omega^{\alpha}_{\mathrm{AB}})^2}\right) \tag{4}$$

States localized on only one fragment C ($\Omega^{\alpha}_{\mathrm{CC}} = \Omega^{\alpha}$) or charge transfer states between two fragments C and D ($\Omega^{\alpha}_{\mathrm{CD}} = \Omega^{\alpha}$, C ≠ D) exhibit $\mathrm{PR}^{\alpha} = 1$. In contrast, for delocalized Frenkel excitonic states or charge resonance states, $PR^{\alpha} > 1$, according to the number of fragments involved. Finally, the weight of charge transfer configurations is determined according to

$$\mathrm{CT}^{\alpha} = \frac{1}{\Omega^{\alpha}}\sum_{\substack{\mathrm{A,B}\\ \mathrm{B}\neq\mathrm{A}}} \Omega^{\alpha}_{\mathrm{AB}} \tag{5}$$

This measure is zero for localized or delocalized Frenkel excitonic states (all off-diagonal elements of $\mathbf{\Omega}^{\alpha}$ are vanishing), whereas it is one for charge transfer or charge resonance states (all diagonal elements of $\mathbf{\Omega}^{\alpha}$ are vanishing). For notational brevity the α superscript, designating the excited state, will be omitted in the following text whenever explicit reference to the state is not needed.

A decomposition of the spectra based on the PR and CT values was performed (see below). The thresholds were chosen to give a meaningful representation of the underlying distribution. PR < 1.5 is seen as fairly localized, whereas PR > 2.5 can be considered as a significantly delocalized state. As a threshold for CT states, CT > 0.5 was chosen, i.e., states that contained at least 50% CT character.

Furthermore, to estimate excitonic couplings between neighboring molecules, a transformation based on the POS value was applied, in analogy to the use of fragment charge differences in charge transfer couplings.[56,57] The model assumes that two adiabatic states ψ^{ad}_i and ψ^{ad}_j are obtained through a unitary transformation applied to two localized diabatic states, positioned on neighboring fragments k and $k+1$

$$\begin{pmatrix}\Psi^{\mathrm{ad}}_i\\ \Psi^{\mathrm{ad}}_j\end{pmatrix} = \mathbf{U}\begin{pmatrix}\Psi^{\mathrm{loc}}_k\\ \Psi^{\mathrm{loc}}_{k+1}\end{pmatrix} \tag{6}$$

$$\mathbf{U} = \begin{pmatrix}\cos(\eta) & -\sin(\eta)\\ \sin(\eta) & \cos(\eta)\end{pmatrix} \tag{7}$$

The POS values of ψ^{loc}_k and $\psi^{\mathrm{loc}}_{k+1}$ are k and $k+1$, respectively, by definition. The values for the adiabatic states (POS^i, POS^j) are obtained by the transformation

$$\begin{pmatrix} \mathrm{POS}^{i} & \mathrm{POS}^{ij} \\ \mathrm{POS}^{ij} & \mathrm{POS}^{j} \end{pmatrix} = \mathbf{U}^{-1}\begin{pmatrix} k & 0 \\ 0 & k+1 \end{pmatrix}\mathbf{U} \tag{8}$$

which can be explicitly rewritten as

$$2k + 1 - \mathrm{POS}^{i} = \mathrm{POS}^{j} = k + \cos^{2}(\eta) \tag{9}$$

To apply this model for extracting diabatic couplings from the quantum chemical computations, it was first necessary to identify pairs of states ψ_i^{ad} and ψ_j^{ad}, which approximately satisfied the underlying assumption of the model. The condition for this was that the left side of equation eq 9 was satisfied for these states, as well as that these states had similar PR and CT values and orbital contributions to the electronic transition. Then eq 9 was applied to compute η and subsequently $\mathbf{U}$. Then, the diabatic localized Hamiltonian $\mathbf{H}^{\mathrm{loc}}$ was computed by transforming the diagonal matrix containing the adiabatic energies of the two states (E_i, E_j)

$$\mathbf{H}^{\mathrm{loc}} = \mathbf{U}\begin{pmatrix} E_i & 0 \\ 0 & E_j \end{pmatrix}\mathbf{U}^{-1}. \tag{10}$$

The excitonic coupling between the localized states H_{if} (i.e., the off-diagonal element of $\mathbf{H}^{\mathrm{loc}}$) is explicitely given as

$$H_{\mathrm{if}} = \cos(\eta)\,\sin(\eta)(E_i - E_j) \tag{11}$$

Molecular visualization and graphical analysis were primarily performed with the PyMOL,[58] VMD,[59] and Jmol[60] packages.

3. RESULTS AND DISCUSSION

3.1. Poly(dAdT)·(dAdT) Duplexes. Figure 2 shows the computed spectra (solid lines) of AT and TATA stacked complexes in vacuo. In both cases a broad peak around 5.5 eV is found in the spectrum. The maximum is located at somewhat higher energies in the tetramer. For comparison, also the total density of transitions (dotted lines), i.e., the spectrum without weighting by the oscillator strengths, is shown to highlight the dark states. This second distribution is significantly broader, which means that there are hidden dark states both at lower and at higher energies than the main contributions of the bright states. States with significant charge transfer character (CT > 0.5) only play a minor role in the absorption spectrum, which means that they cannot be directly excited by UV light. In the DOT charge transfer states are present in the range of 6.0−6.5 eV and a more detailed analysis shows that in the tetramer about 13% of the states considered exhibit CT > 0.5. However, these states are lying at energies above the first absorption maximum. In the dimer spectrum almost no delocalized states (PR > 1.5) are present. In the tetramer spectrum these account also for only about 15% of the states. However, due to their larger oscillator strengths (i.e., the intensity of the PR > 1.5 contribution to the spectrum is significantly larger than the respective contribution to the density of transitions) they are responsible for almost half of the intensity at the absorption maximum. Larger oscillator strengths were to be expected, considering that according to Förster theory brighter states should interact stronger and should therefore also yield more delocalized excitons. At the red and blue edges of the spectrum, the relative importance of delocalized states is significantly diminished. Furthermore, there are almost no excited states (<1%) with a delocalization over more than two and a half bases (PR > 2.5).

In Figure 3 the spectra of the AT and the TATA stacks embedded in the poly(dAdT)·(dAdT) duplex are shown. These spectra are red-shifted by ∼0.3−0.5 eV with respect to the complexes in vacuo, and again the tetramer spectrum is at somewhat higher energies than that of the dimer. Compared to the DOT shown in Figure 2, there are no low-energy dark

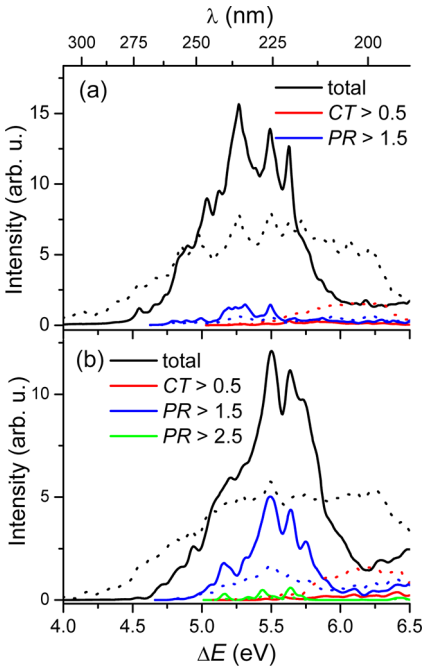

Figure 2. Decomposition of the absorption spectra (solid lines) and densities of transition (dotted lines) of an AT (a) and a TATA (b) nucleobase stack in vacuo.

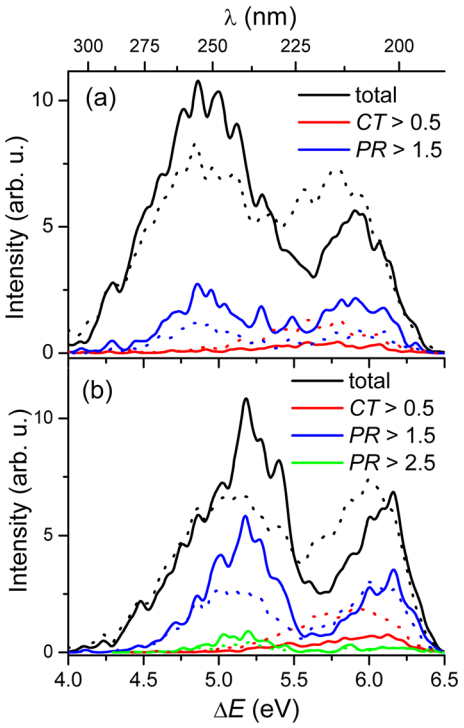

Figure 3. Decomposition of the QM/MM absorption spectra (solid lines) and densities of transition (dotted lines) of an AT (a) and a TATA (b) base stack embedded in a $(\mathrm{dAdT})_6\cdot(\mathrm{dAdT})_6$ duplex.

dx.doi.org/10.1021/jp304725r | J. Phys. Chem. A 2012, 116, 11151−11160

states found now. This is probably due to the fact that nπ^* transitions are blue-shifted by hydrogen bonding and are now located in the energy range of the bright $\pi\pi^*$ states. The maximum of the tetramer QM/MM spectrum lies at 5.2 eV (240 nm). This is about 0.5 eV higher than the experimental maximum of the poly(dAdT)·(dAdT) duplex.[61] In Figure 3 also a second peak in the lower wavelength UV range is visible, cf. ref 61. This difference to the vacuum spectrum (Figure 2) relates to the fact that the high energy area is not completely sampled with the limited number of excited states considered here. Due to a different state ordering, apparently more high energy bright states are included in the QM/MM simulation, whereas in vacuo more dark states are present. To support this hypothesis, we have verified that the second peak emerges also in vacuo if more states are considered. However, because we wanted to concentrate on the first absorption band, the full sampling of the second band, which would also involve substantially higher computational cost, is not further pursued. Charge transfer states play a secondary role even in the spectra, including the DNA environment; they have lower oscillator strengths and are located at higher energies relative to the first absorption peak. In DNA, delocalized states play a somewhat more important role as compared to the spectra in-vacuo. About 30% of the states show PR > 1.5 and because of their higher oscillator strengths, these amount to more than half of the intensity at the absorption maximum of the tetramer. In most cases considered, they extend over neighboring adenine and thymine bases, rather than second neighboring bases of the same kind. In other words: introducing a thymine spacer almost completely decouples the two adenine bases.[62] There are almost no states with PR > 2.5 (about 3%), which means that the majority of the excited states are at most delocalized between two bases. Figure 4 shows the distribution of the CT

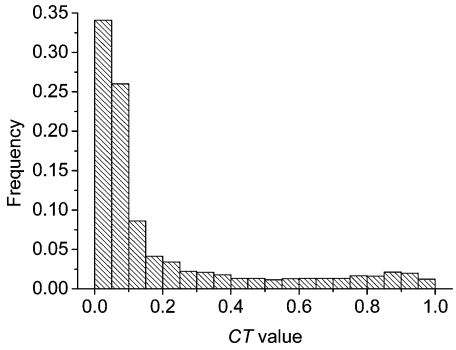

Figure 4. Distribution of CT values in the absorption spectrum of a TATA base stack embedded in a $(dAdT)_6$·$(dAdT)_6$ duplex.

values in the spectrum of the embedded TATA stack. About 60% of the excited states considered exhibit CT < 0.1. Then, states with a strong mixing between locally excited and charge transfer contributions follow (i.e., the CT value is neither close to zero corresponding to only locally excited configurations nor close to one indicating a pure CT state), and about 15% of the states exhibit significant charge separation (CT > 0.5). It should be noted that a simple Frenkel exciton model, neglecting charge transfer interactions, may be insufficient to describe these last 40% of the states.

To get more insight into the character of the excited states, one representative configuration of the embedded TATA stack was analyzed in more detail (Table 1). Aside from the excitation energies and oscillator strengths, the descriptors for position (POS), excitonic participation ratio (PR), and charge transfer (CT) character are given. The type of the excited state is assigned as well. The lowest excited state (S_1) at this configuration is an nπ^* state of the thymine at position three (T3). S_2 and S_3 amount to a pair of excitonic states formed of the $\pi\pi^*$ state of the other thymine residue (T1) and the $\pi\pi^*$ (the bright L_a) state of the adjacent adenine (A2). They are separated by a gap of 0.154 eV. Using eq 11, this amounts to an interchromophore coupling of about 0.065 eV. This large value is consistent with the substantial oscillator strength of S_3 (0.242). The $\pi\pi^*$ (L_b) state of A2 remains fairly isolated at S_7. The two $\pi\pi^*$ states of A4 couple with the $\pi\pi^*$ state of T3 to form three delocalized excitonic states: S_4, S_5, and S_9. Above 5.5 eV, two charge transfer states are present: S_{11} ($A2^+T3^-$) and S_{13} ($A4^+T3^-$). Aside from the states mentioned, there is a large number of localized nπ^* states. Furthermore, S_{18} and S_{19} form a pair of delocalized nπ^* states, probably due to an accidental degeneracy, separated by 0.020 eV (with a coupling of about 0.009 eV). To estimate the effects of environment, the excited states of the isolated molecule at the same geometry were computed as well. Electronic states computed in DNA environment and in vacuo were related to each other on the basis of the analysis of the electronic wave function, and wherever this was possible, the energy of the corresponding isolated state ($\Delta E_{SV,isol}$) is given as well in Table 1. However, in some cases different resonances and thus different delocalization degrees were present in the two calculations, not allowing a clear assignment. To give information about these states, a table with the full information is presented in the Supporting Information (Table S1). It can be observed that the DNA environment significantly destabilizes all the nπ^* states (by about 0.4 eV). This strong shift is due to hydrogen bonding interactions and agrees well with previous experience.[63−65] The $\pi\pi^*$ states seem largely unaffected by environmental effects, and no clear trend is present here. The vertical excitation energies of the charge transfer states are almost not affected here. However, it should be noted that they might be somewhat stabilized by an environmental model including the electronic response of the environment to the excitation, cf. refs 21 and 25. For comparison, also a calculation at the same molecular geometry was performed where only the central AT was considered in the QM region and the outer two bases were included in the MM region (Table S2, Supporting Information). For many of the resulting dimer states a clear assignment to the tetramer states was possible. Most of the tetramer states were blue-shifted by about 0.1−0.2 eV with respect to the embedded dimers, which is a trend also observed in Figures 2 and 3. This suggests that the stacking interaction in DNA slightly affects the excited states through an interaction term, which is not included in the electrostatic embedding model (cf. ref 66. for a discussion of these terms).

Next, the reasons for spectral broadening in the poly(dAdT)·(dAdT) duplex are examined. In particular, the contributions of environmental fluctuations and intra- and intermolecular motions will be analyzed, and the effect of quantum mechanical zero-point vibrations will be highlighted. Initially, the first absorption band of a stack in vacuo with fixed intermolecular degrees of freedom (Figure 2) and the QM/MM simulation, where also interbase motions are considered (Figure 3), are compared. It can be seen that aside from the general overall shift, the peak shapes are very similar. This already suggests that intramolecular motions are the decisive factor in spectral broadening, whereas both interbase motions

Table 1. Excitation Energies (ΔE, eV), Oscillator Strengths (f), Statistical Descriptors, and Type Assignments at the ADC(2)/SV Level for the First 20 Excited States of a TATA Base Stack (Designated T1, A2, T3, A4) Embedded in a $(dAdT)_6{\cdot}(dAdT)_6$ Duplex Solvated in Water Computed at One Selected Geometry

state	ΔE_{SV}	f	POS	PR	CT	type	$\Delta E_{SV,isol}$[a]	ΔE_{SVP}[b]
S_1	4.679	0.001	2.99	1.04	0.03	n(T3)−π^*(T3)	4.261	4.453
S_2	4.833	0.052	1.79	**1.63**	0.02	π(A2)−π^*(A2)/π(T1)−π^*(T1)	4.823[c]	4.604
S_3	4.986	**0.242**	1.29	**1.63**	0.02	π(T1)−π^*(T1)/π(A2)−π^*(A2)	5.242[c]	4.768
S_4	5.039	0.027	3.31	**2.35**	0.07	π(T3)−π^*(T3)/π(A4)−π^*(A4)	5.161[c]	4.824
S_5	5.095	0.029	3.69	**1.63**	0.04	π(A4)−π^*(A4)/π(T3)−π^*(T3)	5.044[c]	4.935
S_6	5.121	0.017	1.06	1.13	0.02	n(T1)−π^*(T1)	4.718	4.925
S_7	5.150	0.033	2.11	1.42	0.05	π(A2)−π^*(A2)	5.112[c]	4.981[c]
S_8	5.193	0.002	2.04	1.06	0.03	n(A2)−π^*(A2)	4.752	5.118
S_9	5.265	**0.283**	3.73	**1.60**	0.04	π(A4)−π^*(A4)/π(T3)−π^*(T3)	5.317[c]	5.012[c]
S_{10}	5.330	0.029	3.98	1.04	0.02	n(A4)−π^*(A4)	4.779	5.230
S_{11}	5.559	0.005	2.52	1.08	**0.95**	π(A2)−π^*(T3)	5.581	5.208
S_{12}	5.583	0.000	3.00	1.04	0.03	n(T3)−π^*(T3)	5.239	5.248
S_{13}	5.700	0.014	3.39	1.26	**0.81**	π(A4)−π^*(T3)	5.665	5.388
S_{14}	5.937	0.010	1.04	1.06	0.06	n(T1)−π^*(T1)	5.742	5.644
S_{15}	6.127	0.021	3.06	1.21	0.17	n(T3)−π^*(T3)		5.742
S_{16}	6.175	0.022	4.00	1.01	0.01	n(A4)−π^*(A4)	5.671	
S_{17}	6.214	0.012	1.95	1.16	0.14	n(A2)−π^*(A2)	5.898	
S_{18}	6.248	0.005	2.33	**1.83**	0.08	n(A2)−π^*(A2)/n(T3)−π^*(T3)	5.812[c]	
S_{19}	6.267	0.021	2.69	**2.01**	0.10	n(T3)−π^*(T3)/n(A2)−π^*(A2)		
S_{20}	6.332	**0.150**	1.52	**1.76**	0.17	π(T1)−π^*(T1)/π(A2)−π^*(A2)		

[a]ADC(2)/SV excitation energy of the corresponding state in the isolated tetramer of the same geometry. [b]QM/MM excitation energy of the corresponding state at the ADC(2)/SVP level. [c]Only an approximate assignment was possible.

and environmental motions play only a minor role in this context. To get a more detailed insight into this phenomenon, a spectrum of AT in DNA with frozen intramolecular degrees of freedom was computed (Figure 5a). This was achieved by replacing the adenine and thymine fragments of the QM part in each MD snapshot with the ground-state equilibrium geometries of the adenine and thymine molecules. For each of these structures the electronic excitations were computed. In this way the computed spectrum included solvent and backbone rearrangements, as well as relative base−base movements, but no intramolecular motions of the bases. The resulting spectrum looks completely different as compared to the full simulation (Figure 3a). The broad peak is now split into three well-separated components, corresponding to the adenine $\pi\pi^*$ (L_b), thymine $\pi\pi^*$, and adenine $\pi\pi^*$ (L_a) states. The spectral broadening for these peaks is on the order of only about 0.1 eV. Next we examined the result obtained when only classical contributions to intramolecular motions are considered, i.e., the calculation of electronic excitations is directly performed at the configuration of the MD snapshot without considering the quantum mechanical zero point vibrations (Figure 5b). In this case, the state energies overlap again, forming one broad peak. However, the result is significantly different from the full simulation (Figure 3a). The peak is blue-shifted by about 0.5 eV, and additionally, its shape is completely different with a somewhat narrower peak and a broad plateau. In summary, we can conclude that intramolecular motions, resulting from quantum mechanical zero-point vibrations, are the dominant factor in determining the spectral shape, which is in line with the experimental observation that the spectrum of the duplex is very similar to the sum of its constituents.[61] These vibrations should be active also after UV absorption, and the strong coupling to the excited states could lead to subpicosecond excitation energy transfer between the bases as suggested from experimental investigations.[11,15]

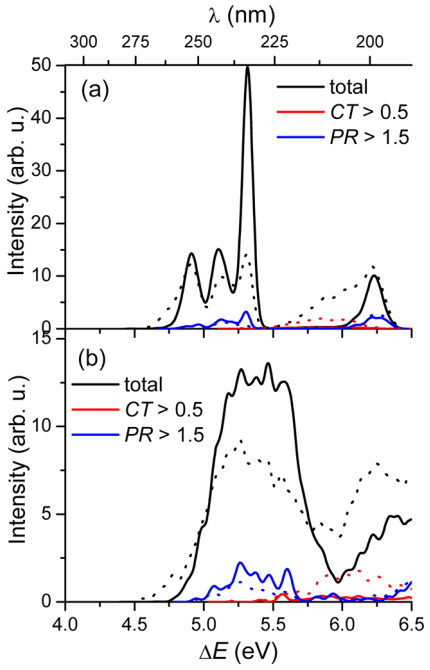

Figure 5. Decomposition of the QM/MM absorption spectra (solid lines) and densities of transition (dotted lines) of an AT base stack embedded in a $(dAdT)_6{\cdot}(dAdT)_6$ duplex with frozen intramolecular coordinates (a) and only consideration of the classical contributions to intramolecular motions (b).

QM/MM excitation energies were also computed for the TATA tetramer at the ADC(2) level using the SVP basis containing polarization functions. Respective ΔE_{SVP} values are given in the last column of Table 1. There is a general decrease of about 0.2 eV found for the SVP results in comparison to the

SV data. Aside from that, the results are consistent, and in particular the state orderings are almost identical. Some slight deviations are observed for the nπ^* states on adenine, which are affected somewhat less than average, and the CT states, which are red-shifted a bit more. To get more statistical insight, the QM/MM spectrum of the embedded AT stack (Figure 3a) was recomputed at the ADC(2)/SVP level (Figure 6). The two

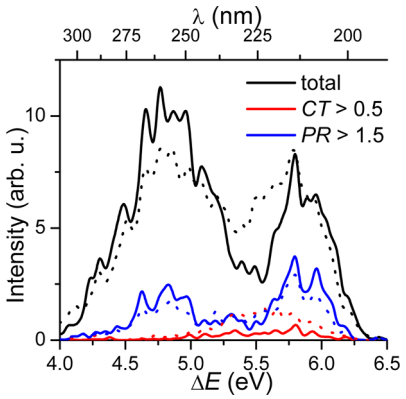

Figure 6. Decomposition of the QM/MM absorption spectrum (solid lines) and density of transition (dotted lines) of an AT base stack embedded in a $(dAdT)_6{\cdot}(dAdT)_6$ duplex, computed at the ADC(2)/SVP level.

figures agree well in all main features (peak positions, peak heights, and distribution into the different components); it is only found that the SVP spectrum is shifted to lower energies by about 0.1 or 0.2 eV as observed for the calculation reported in Table 1. In summar, it can be concluded that basis set effects should not play a large role in the general interpretation of the spectra except for the fact that excitation energies are overestimated by about 0.2 eV as compared to SVP and probably somewhat more as compared to the complete basis set limit. In this sense, the shift of 0.5 eV with respect to the experimental absorption spectrum[61] is probably to a large part due to basis set effects.

3.2. Poly(dGdC)·(dGdC) Duplexes. The spectra for the GC and the CGCG stacks in vacuo are shown in Figure 7. Compared to those for the adenine−thymine stacks, they are significantly broader. However, the decomposition of the spectra into their different contributions is similar to the corresponding ones of the adenine−thymine case. Charge transfer states (CT > 0.5) again play only a minor role (10% in the tetramer) and are located at higher energies. Just as in the TATA case only a small fraction of the excited states are delocalized; e.g., in the tetramer only about 13% of the excited states considered show PR > 1.5. Again, these have oscillator strengths somewhat higher than average, which can be seen from the fact that the spectrum lies above the normalized DOT, in accordance with Förster theory. However, as opposed to the TATA case the enhancement is not as strong and only about a third of the intensity at the absorption maximum is due to delocalized states.

After GC and CGCG, respectively, are embedded into the hydrated duplex, the shape of the absorption spectra is somewhat altered (Figure 8) and the spectra exhibit more pronounced peaks at the center of the band. In the tetramer spectrum the absorption maximum is located at about 5.4 eV (230 nm), which is ∼0.5 eV above the experimental value.[14] Charge transfer states play only a minor role and are located in

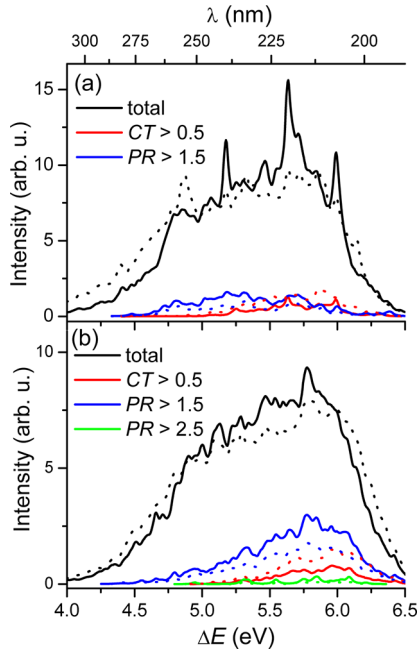

Figure 7. Decomposition of the absorption spectra (solid lines) and densities of transition (dotted lines) of a GC (a) and a CGCG (b) base stack in vacuo.

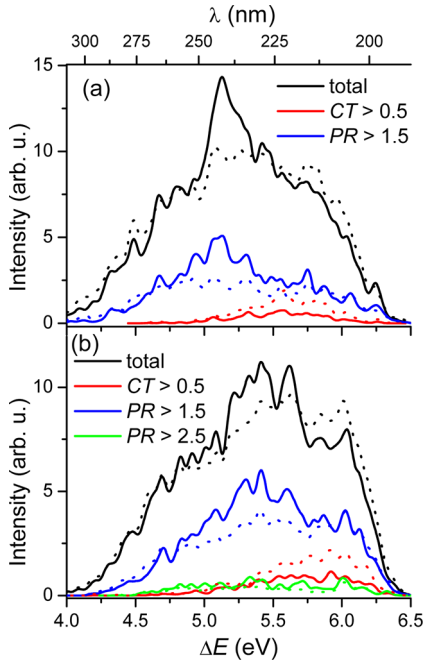

Figure 8. Decomposition of the QM/MM absorption spectra (solid lines) and densities of transition (dotted lines) of an GC (a) and a CGCG (b) base stack embedded in a $(dGdC)_6{\cdot}(dGdC)_6$ duplex.

the high energy part of the spectrum. States delocalized over two bases are more pronounced as compared to the spectra in vacuo: in the tetramer 37% of the excited states show PR > 1.5 (as opposed to 13% in vacuo). They peak at the absorption maximum, where they make up about half of the intensity. Again, there are almost no states (only about 4%) with three bases participating (PR > 2.5). At the red edge of the spectrum, the states are mostly localized on one base. The distribution of CT values of the embedded tetramer is presented in Figure 9.

dx.doi.org/10.1021/jp304725r | J. Phys. Chem. A 2012, 116, 11151−11160

About 50% of the states show Frenkel excitonic character (CT < 0.1) and there are about 12% true charge transfer states (CT > 0.5).

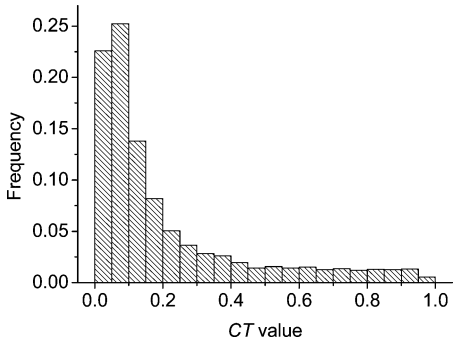

Figure 9. Distribution of CT values in the absorption spectrum of a CGCG base stack stack embedded in a $(dGdC)_6{\cdot}(dGdC)_6$ duplex.

A detailed analysis of the excited states at one representative configuration of the embedded CGCG stack is shown in Table 2. The four lowest excited states are formed from $\pi\pi^*$ states on the four bases. The S_1 and S_2 excitations are located on the neighboring guanine G4 and cytosine C3 residues, respectively. S_3 and S_4 form a resonant pair on C1 and G2 separated by a gap of 0.072 eV, which according to eq 11 corresponds to a coupling of about 0.030 eV. The S_5 and S_{10} states are $n\pi^*$ states localized on the cytosine residues. S_6, S_7, S_9, and S_{13} form a set of four localized $\pi\pi^*$ states on the four bases. The lowest lying charge transfer state (S_8), in the direction from G2 to C3, is located at an excitation energy of 5.284 eV. S_{11} and S_{12} comprise a set of weakly coupled (<0.001 eV) $n\pi^*$ states, which are delocalized due to the fact that their site energies are by chance nearly degenerate. Two localized states follow. S_{15} and S_{16} again derive from a pair of nearly degenerate $n\pi^*$ states, which are somewhat more strongly coupled (0.007 eV). S_{17} is the next charge transfer state, followed by three localized states. An excited-state calculation was performed for the same geometry in vacuo as well. A direct relation to the states computed at QM/MM level was not always possible because different mixings between configurations were obtained. Wherever possible, this value is given in Table 2 ($\Delta E_{SV,isol}$). Just like for TATA, it can be observed that the $n\pi^*$ states are strongly destabilized by solvation and hydrogen bonding (by about 0.5 eV). In contrast, the $\pi\pi^*$ states deviate in both directions and respective shifts are not quite as pronounced. The charge transfer state (S_8) was found at about the same energy in the isolated complex. To test for basis set effects, the QM/MM energies at the ADC(2)/SVP (ΔE_{SVP}) were computed (Table 2). Again, there is a general quite consistent decrease of about 0.2 eV found for ΔE_{SVP} (last column) as opposed to those of the SV results (second column). It appears that the charge transfer states are red-shifted a bit more (0.3 eV).

3.3. Excitonic Delocalization and Charge Transfer. A major outcome of our study based on sampling of intra- and intermolecular vibrational modes is that in alternating duplexes excited states are mostly localized between two neighboring bases. A previous TDDFT study provided similar results for poly dAdT[20] and rather low delocalization degrees for this system were also reported from experiment.[12] Estimates for poly dGdC by another group range from at least two[23] to six or eight bases.[18] These authors point out that their results in alternating poly dGdC were similar to those in homopolymeric poly dA. For this latter system quite divergent delocalization degrees from two or three[12,20,22,27] to six or eight[16,18] monomer units were reported. Our calculations show quite conclusively that at least for alternating duplexes the lower estimates are

Table 2. Excitation Energies (ΔE, eV), Oscillator Strengths (f), Statistical Descriptors, and Type Assignments at the ADC(2)/SV Level for the First 20 Excited States of a CGCG Base Stack (Designated C1, G2, C3, G4) Embedded in a $(dGdC)_6{\cdot}(dGdC)_6$ Duplex Solvated in Water Computed at One Selected Geometry

state	ΔE_{SV}	f	POS	PR	CT	type	$\Delta E_{SV,isol}$[a]	ΔE_{SVP}[b]
S_1	4.619	**0.135**	3.99	1.02	0.02	π(G4)−π^*(G4)	4.579	4.479
S_2	4.719	0.019	2.96	1.14	0.12	π(C3)−π^*(C3)	4.421	4.520
S_3	4.804	0.003	1.23	**1.54**	0.07	π(C1)−π^*(C1)/π(G2)−π^*(G2)	4.510[c]	4.642
S_4	4.876	**0.121**	1.81	**1.68**	0.06	π(G2)−π^*(G2)/π(C1)−π^*(C1)	4.913[c]	4.703
S_5	4.971	0.020	3.01	1.13	0.09	n(C3)−π^*(C3)		4.781
S_6	5.167	**0.227**	3.92	1.17	0.03	π(G4)−π^*(G4)	5.191[c]	4.932
S_7	5.269	**0.178**	1.06	1.11	0.07	π(C1)−π^*(C1)		5.051
S_8	5.284	0.050	2.56	1.23	**0.87**	π(G2)−π^*(C3)	5.343	4.980
S_9	5.358	0.080	3.04	1.24	0.14	π(C3)−π^*(C3)		5.078
S_{10}	5.475	0.008	1.05	1.08	0.05	n(C1)−π^*(C1)	5.107	5.246
S_{11}	5.553	0.005	3.69	**1.68**	0.02	n(G4)−π^*(G4)/n(C3)−π^*(C3)	4.830[c]	5.350[c]
S_{12}	5.554	0.014	3.20	**1.61**	0.04	n(C3)−π^*(C3)/n(G4)−π^*(G4)		5.288[c]
S_{13}	5.558	**0.184**	2.09	1.47	0.08	π(G2)−π^*(G2)	5.514[c]	5.293
S_{14}	5.661	0.029	2.98	1.12	0.07	n(C3)−π^*(C3)	5.070	5.455
S_{15}	5.676	0.012	1.18	1.41	0.05	n(C1)−π^*(C1)/n(G2)−π^*(G2)	4.918[c]	5.506
S_{16}	5.693	0.002	1.82	**1.51**	0.07	n(G2)−π^*(G2)/n(C1)−π^*(C1)	5.185[c]	5.483
S_{17}	5.784	0.002	3.44	1.15	**0.89**	π(G4)−π^*(C3)		5.526
S_{18}	5.824	**0.423**	1.10	1.19	0.08	π(C1)−π^*(C1)		5.602
S_{19}	5.921	0.073	1.06	1.10	0.08	π(C1)−π^*(C1)		5.739
S_{20}	6.025	**0.327**	3.00	1.23	0.13	π(C3)−π^*(C3)		

[a]ADC(2)/SV excitation energy of the corresponding state in the isolated tetramer of the same geometry. [b]QM/MM excitation energy of the corresponding state at the ADC(2)/SVP level. [c]Only an approximate assignment was possible.

more realistic. The hypothesis of rather localized states is also in agreement with the observation that excited-state lifetimes are nearly independent of the helix conformation and the base-pairing motif in $d(GC)_9 \cdot d(GC)_9$.[67] Evidence for subpicosecond energy transfer, which has been obtained from fluorescence anisotropy studies, was seen as an indication for strongly delocalized states.[15] However, the strong coupling between the electronic-state energies and intramolecular motions (as seen in Figure 5) indicates that energy transfer is not a purely electronic process but strongly correlated to intramolecular vibrations, which operate on just that ultrafast time scale.

The computation of charge transfer states is a challenge with any computational strategy. Particular problems are the failure of standard TDDFT functionals and the necessity for a high level description of environmental polarization, cf. ref 29. An initial TDDFT study of poly dA placed charge transfer states well below the localized and Frenkel excitonic states.[24] However, this behavior was later attributed to the insufficiency of PBE0 in describing charge transfer states, and subsequent TDDFT,[20,25] complete active space perturbation-theory to second-order (CASPT2)[17] and RI-CC2[26] studies found charge transfer states at about the same energy as the lowest $\pi\pi^*$ transitions or somewhat higher, in accordance with our current investigations. It is interesting to note that the relative position of the charge transfer states is found to be quite independent of the model used in our calculations (vacuum or QM/MM, dimer or tetramer). Thus, Coulomb effects of the DNA environment and in particular the extra degree of dynamic polarizability, present through the additional bases in the tetramer, does not significantly alter the energy of the charge transfer states. Moreover, our above results suggest that differential basis set effects should only have a small impact on CT states (0.1 eV). To estimate the magnitude of stabilization of the CT states due to electronic polarization not explicitly included in our force field, one could consider results reported from calculations using a polarizable continuum model (PCM). In linear-response PCM calculations for water and other solvents only small red shifts (0.1−0.2 eV) were obtained.[26] A somewhat larger value was reported when the state-specific PCM was used in aqueous solution, where an additional stabilization energy of 0.5 eV, resulting from the state-specific solvation, was computed.[21,25] However, for partially charge separated states as they occur in the present investigations (cf. Figures 4 and 9) and considering the fact that the dielectric constant of water is certainly an upper limit for the local dielectric constant in DNA, the actual shift may well be smaller even though a conclusive answer is still to be found. Whereas charge transfer states thus appear to be located at higher energies in the Franck−Condon region, they may well be stabilized in the dynamical processes after photoexcitation, e.g., through interbase motions[68] or solvent reorganization. The strong mixing between Frenkel and CT states, which can be deduced from the fact that there is a wide range of such mixed states ($0.1 < CT < 0.9$ in Figure 4 and Figure 9), could provide a direct route from the bright states into trapped charge transfer states by dynamical charge separation, see also refs.[21,28,68−70]

4. CONCLUSIONS

Extended atomistic simulations of the UV absorption spectrum of $(dAdT)_6 \cdot (dAdT)_6$ and $(dGdC)_6 \cdot (dGdC)_6$ alternating duplexes, respectively, have been performed using a QM/MM scheme with an extended QM part including four stacked nucleobases in the central region of the duplex. As the quantum chemical method the RI-ADC(2) method has been chosen, which is free of artifacts concerning charge transfer states and is supposed to provide, within the possibilities of computational methods available for the relatively large molecular systems encountered here, a balanced description of these states in comparison to locally excited and delocalized excitonic states.

On the basis of these calculations our main conclusions about the properties of the absorbing states in alternating duplexes are

- In the majority of the cases, the excited states are localized on either one or two nucleobases. The computed distribution of delocalized states is peaking at the absorption maximum.
- In the Franck−Condon region, i.e., the configurational space immediately accessed after UV absorption, charge transfer states are located in the higher energy range of the spectrum somewhat above the major portion of the energy distribution of the bright states.
- There is a significant coupling between locally excited and charge separated states, yielding a large number of states of partial CT character. This could provide a route to dynamical charge separation and excimer formation.
- Spectral broadening leading to one broad peak is largely caused by intramolecular vibrations. In other words, there is a strong electron−phonon coupling between intramolecular vibrations and excited-state energies. This suggests that even the first ultrafast processes are coupled to nuclear vibrations and no purely electronic dynamics is present.

■ ASSOCIATED CONTENT

Supporting Information

Detailed analysis of a calculation of the TATA stack in vacuo (Table S1) and of a QM/MM calculation considering only the central AT stack in the QM region (Table S2), geometries and total energies of the isolated dimer and tetramer stacks (Tables S3−S6). This material is available free of charge via the Internet at http://pubs.acs.org.

■ AUTHOR INFORMATION

Corresponding Author

*E-mail: felix.plasser@univie.ac.at (F.P.), hans.lischka@ttu.edu (H.L.).

Notes

The authors declare no competing financial interest.

■ ACKNOWLEDGMENTS

This work has been supported by the Austrian Science Fund within the framework of the Special Research Program and F41 Vienna Computational Materials Laboratory (ViCoM). This work was also performed as part of research supported by the National Science Foundation Partnership in International Research and Education (PIRE) Grant No. OISE-0730114. Support was also provided by the Robert A. Welch Foundation under Grant No. D-0005. The calculations were performed at the Vienna Scientific Cluster (project nos. 70019 and 70151). F.P. is a recipient of a DOC fellowship of the Austrian Academy of Sciences.

■ REFERENCES

(1) Pfeifer, G. P.; You, Y. H.; Besaratinia, A. *Mutat. Res., Fundam. Mol. Mech. Mutagen.* **2005**, *571*, 19.

(2) Ullrich, S.; Schultz, T.; Zgierski, M. Z.; Stolow, A. *Phys. Chem. Chem. Phys.* **2004**, *6*, 2796.
(3) Perun, S.; Sobolewski, A. L.; Domcke, W. *J. Am. Chem. Soc.* **2005**, *127*, 6257.
(4) Canuel, C.; Mons, M.; Piuzzi, F.; Tardivel, B.; Dimicoli, I.; Elhanine, M. *J. Chem. Phys.* **2005**, *122*, 074316.
(5) Marian, C. M. *J. Chem. Phys.* **2005**, *122*, 104314.
(6) Merchan, M.; Gonzalez-Luque, R.; Climent, T.; Serrano-Andres, L.; Rodriuguez, E.; Reguero, M.; Pelaez, D. *J. Phys. Chem. B* **2006**, *110*, 26471.
(7) Hudock, H. R.; Levine, B. G.; Thompson, A. L.; Satzger, H.; Townsend, D.; Gador, N.; Ullrich, S.; Stolow, A.; Martinez, T. J. *J. Phys. Chem. A* **2007**, *111*, 8500.
(8) Middleton, C. T.; de La Harpe, K.; Su, C.; Law, Y. K.; Crespo-Hernandez, C. E.; Kohler, B. *Annu. Rev. Phys. Chem.* **2009**, *60*, 217.
(9) Barbatti, M.; Aquino, A. J. A.; Szymczak, J. J.; Nachtigallová, D.; Hobza, P.; Lischka, H. *Proc. Natl. Acad. Sci. U. S. A.* **2010**, *107*, 21453.
(10) Crespo-Hernandez, C.; Cohen, B.; Kohler, B. *Nature* **2005**, *436*, 1141.
(11) Kwok, W. M.; Ma, C. S.; Phillips, D. L. *J. Am. Chem. Soc.* **2006**, *128*, 11894.
(12) Buchvarov, I.; Wang, Q.; Raytchev, M.; Trifonov, A.; Fiebig, T. *Proc. Natl. Acad. Sci. U. S. A.* **2007**, *104*, 4794.
(13) Markovitsi, D.; Gustavsson, T.; Talbot, F. *Photochem. Photobiol. Sci.* **2007**, *6*, 717.
(14) Vaya, I.; Miannay, F.; Gustavsson, T.; Markovitsi, D. *ChemPhysChem* **2010**, *11*, 987.
(15) Onidas, D.; Gustavsson, T.; Lazzarotto, E.; Markovitsi, D. *Phys. Chem. Chem. Phys.* **2007**, *9*, 5143.
(16) Czader, A.; Bittner, E. R. *J. Chem. Phys.* **2008**, *128*, 035101.
(17) Olaso-Gonzalez, G.; Merchan, M.; Serrano-Andres, L. *J. Am. Chem. Soc.* **2009**, *131*, 4368.
(18) Markovitsi, D.; Gustavsson, T.; Banyasz, A. *Mutat. Res., Rev. Mutat. Res.* **2010**, *704*, 21.
(19) Takaya, T.; Su, C.; de La Harpe, K.; Crespo-Hernandez, C.; Kohler, B. *Proc. Natl. Acad. Sci. U. S. A.* **2008**, *105*, 10285.
(20) Lange, A.; Herbert, J. *J. Am. Chem. Soc.* **2009**, *131*, 3913.
(21) Santoro, F.; Barone, V.; Lami, A.; Improta, R. *Phys. Chem. Chem. Phys.* **2010**, *12*, 4934.
(22) Tonzani, S.; Schatz, G. C. *J. Am. Chem. Soc.* **2008**, *130*, 7607.
(23) Emanuele, E.; Zakrzewska, K.; Markovitsi, D.; Lavery, R.; Millie, P. *J. Phys. Chem. B* **2005**, *109*, 16109.
(24) Santoro, F.; Barone, V.; Improta, R. *Proc. Natl. Acad. Sci. U. S. A.* **2007**, *104*, 9931.
(25) Santoro, F.; Barone, V.; Improta, R. *ChemPhysChem* **2008**, *9*, 2531.
(26) Aquino, A. J. A.; Nachtigallova, D.; Hobza, P.; Truhlar, D. G.; Hattig, C.; Lischka, H. *J. Comput. Chem.* **2011**, *32*, 1217.
(27) Emanuele, E.; Markovitsi, D.; Millié, P.; Zakrzewska, K. *ChemPhysChem* **2005**, *6*, 1387.
(28) Bittner, E. R. *J. Photochem. Photobiol., A* **2007**, *190*, 328.
(29) Plasser, F.; Barbatti, M.; Aquino, A. J. A.; Lischka, H. *Theor. Chim. Acta* **2012**, *131*, 1073.
(30) Dreuw, A.; Head-Gordon, M. *J. Am. Chem. Soc.* **2004**, *126*, 4007.
(31) Hieringer, W.; Görling, A. *Chem. Phys. Lett.* **2006**, *419*, 557.
(32) Christiansen, O.; Koch, H.; Jorgensen, P. *Chem. Phys. Lett.* **1995**, *243*, 409.
(33) Trofimov, A. B.; Schirmer, J. *J. Phys. B: At., Mol. Opt. Phys.* **1995**, *28*, 2299.
(34) Hättig, C.; Weigend, F. *J. Chem. Phys.* **2000**, *113*, 5154.
(35) Nachtigallova, D.; Hobza, P.; Ritze, H. *Phys. Chem. Chem. Phys.* **2008**, *10*, 5689.
(36) Kozak, C.; Kistler, K.; Lu, Z.; Matsika, S. *J. Phys. Chem. B* **2010**, *114*, 1674.
(37) Kubar, T.; Elstner, M. *J. Phys. Chem. B* **2008**, *112*, 8788.
(38) Hattig, C. *Adv. Quantum Chem.* **2005**, *50*, 37.
(39) Ahlrichs, R.; Bär, M.; Häser, M.; Horn, H.; Kölmel, C. *Chem. Phys. Lett.* **1989**, *162*, 165.
(40) Schafer, A.; Horn, H.; Ahlrichs, R. *J. Chem. Phys.* **1992**, *97*, 2571.
(41) Barbatti, M.; Granucci, G.; Persico, M.; Ruckenbauer, M.; Vazdar, M.; Eckert-Maksic, M.; Lischka, H. *J. Photochem. Photobiol., A* **2007**, *190*, 228.
(42) Karney, C. F. F. *J. Mol. Graph. Model.* **2007**, *25*, 595.
(43) Plasser, F.; Barbatti, M.; Aquino, A. J. A.; Lischka, H. *J. Phys. Chem. A* **2009**, *113*, 8490.
(44) Plasser, F. Dynamics simulation of excited state intramolecular proton transfer (http://othes.univie.ac.at/4414/). *Master Thesis*, 2009.
(45) Ruckenbauer, M.; Barbatti, M.; Muller, T.; Lischka, H. *J. Phys. Chem. A* **2010**, *114*, 6757.
(46) Field, M. J.; Bash, P. A.; Karplus, M. *J. Comput. Chem.* **1990**, *11*, 700.
(47) Bakowies, D.; Thiel, W. *J. Phys. Chem.* **1996**, *100*, 10580.
(48) Nicoll, R. M.; Hindle, S. A.; MacKenzie, G.; Hillier, I. H.; Burton, N. A. *Theor. Chem. Acc.* **2001**, *106*, 105.
(49) Martinez, J. M.; Martinez, L. *J. Comput. Chem.* **2003**, *24*, 819.
(50) Kollman, P. A.; Wang, J. M.; Cieplak, P. *J. Comput. Chem.* **2000**, *21*, 1049.
(51) Ponder, J. W.; Richards, F. M. *J. Comput. Chem.* **1987**, *8*, 1016.
(52) Barbatti, M.; Granucci, G.; Ruckenbauer, M.; Plasser, F.; Pittner, J.; Persico, M.; Lischka, H. *NEWTON-X: a package for Newtonian dynamics close to the crossing seam*, 2011, www.newtonx.org.
(53) Plasser, F.; Lischka, H. *J. Chem. Theory Comput.* **2012**, DOI: 10.1021/ct300307c.
(54) Tretiak, S.; Mukamel, S. *Chem. Rev.* **2002**, *102*, 3171.
(55) Luzanov, A. V.; Zhikol, O. A. *Int. J. Quantum Chem.* **2010**, *110*, 902.
(56) Voityuk, A. A.; Rosch, N. *J. Chem. Phys.* **2002**, *117*, 5607.
(57) Plasser, F.; Lischka, H. *J. Chem. Phys.* **2011**, *134*, 034309.
(58) Schrodinger, L. L. C. *The PyMOL Molecular Graphics System*, Version 1.1 The PyMOL Molecular Graphics System, Version 1.1, 2008.
(59) Humphrey, W.; Dalke, A.; Schulten, K. *J. Mol. Graph.* **1996**, *14*, 33.
(60) Jmol.: an open-source Java viewer for chemical structures in 3D. http://www.jmol.org/.
(61) Markovitsi, D. *Pure Appl. Chem.* **2009**, *81*, 1635.
(62) Nielsen, L. M.; Holm, A. I. S.; Hoffmann, S. V.; Nielsen, S. B. *J. Photochem. Photobiol., A* **2011**, *220*, 1.
(63) Wesolowski, T. A. *J. Am. Chem. Soc.* **2004**, *126*, 11444.
(64) Santoro, F.; Barone, V.; Gustavsson, T.; Improta, R. *J. Am. Chem. Soc.* **2006**, *128*, 16312.
(65) Szymczak, J. J.; Muller, T.; Lischka, H. *Chem. Phys.* **2010**, *375*, 110.
(66) Slavicek, P.; Martinez, T. J. *J. Chem. Phys.* **2006**, *124*, 084107.
(67) de La Harpe, K.; Crespo-Hernandez, C. E.; Kohler, B. *ChemPhysChem* **2009**, *10*, 1421.
(68) Starikov, E. B.; Cuniberti, G.; Tanaka, S. *J. Phys. Chem. B* **2009**, *113*, 10428.
(69) Improta, R.; Santoro, F.; Barone, V.; Lami, A. *J. Phys. Chem. A* **2009**, *113*, 15346.
(70) Improta, R.; Barone, V. *Angew. Chem., Int. Ed.* **2011**, *50*, 12016.